Supplement of Hydrol. Earth Syst. Sci., 28, 1527–1538, 2024
https://doi.org/10.5194/hess-28-1527-2024-supplement

Hydrology and Earth System Sciences
Open Access
EGU

Supplement of

Sediment transport in South Asian rivers high enough to impact satellite gravimetry

Alexandra Klemme et al.

Correspondence to: Alexandra Klemme (aklemme@uni-bremen.de)

1 Evaluation of Himalayan uplift data for regional gravity

The Indian continental plate moves at a speed of about $50\,\mathrm{mm\,yr^{-1}}$ below the Eurasian plate (Bisht et al., 2021; Larson et al., 1999). Over the last 40 million years, this continental collision has created the Himalayan mountain range (Fu and Freymueller, 2012), and since it is still ongoing, the Himalayan arc experiences natural hazards like landslides and earthquakes as well as a continuous uplift (Bisht et al., 2021). Most relevant for our study, this plate collision causes an increase in land mass and consequentially a gravity trend that could impact long-term gravimetry observations.

In order to estimate the impact of this gravity increase on trends in our study, we combine GPS data of Himalayan uplift from three studies (Table S4, Xu et al., 2000; Fu and Freymueller, 2012; Bisht et al., 2021) and derive an estimate for the related mass increase. We include stations that are located within the Ganges and Brahmaputra catchments and interpolate the uplift rates between them (Figure S1). This data yields an average uplift within the catchment mountain ranges of $(4.8 \pm 2.5)\,\mathrm{mm\,yr^{-1}}$. At a mountain rock density of $2.67\,\mathrm{g\,cm^{-3}}$ (Ravikumar et al., 2020; Rao et al., 2022), this represents a gravity increase of $(1.9 \pm 1.0) \cdot 10^{12}\,\mathrm{kg\,yr^{-1}}$ currently not considered when deriving trends in terrestrial water storage (TWS) based on satellite gravimetry.

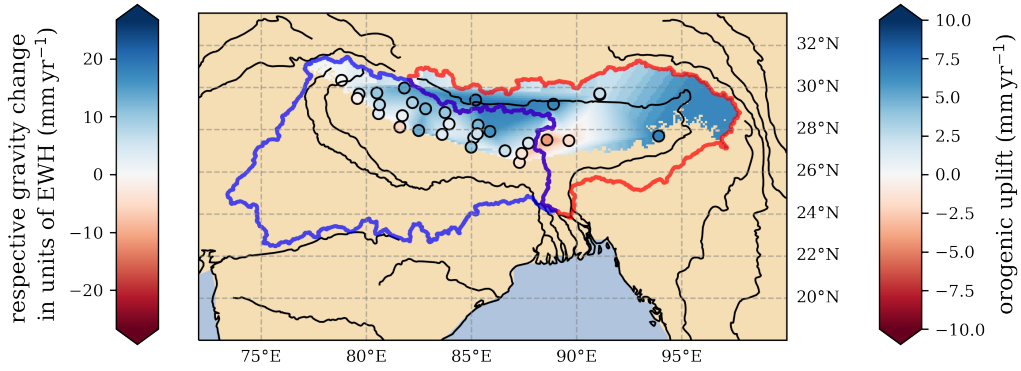

Figure S1. Map of orogenic uplift detected at specific GPS stations (circles) in the Ganges and Brahmaputra mountain region as well as regional uplift data based on interpolation of such station data (shaded area). Station GPS data and literature sources are listed in Table S4. The right color bar indicates the actual uplift, while the left color bar shows the corresponding impact on gravity change in units of equivalent water height (EWH) based on an average rock density of $2.67\,\mathrm{g\,cm^{-3}}$.

Attempting to separate the mass change within the two catchments yields an average uplift of $5.4\,\mathrm{mm\,yr^{-1}}$ in the Ganges mountains and $4.6\,\mathrm{mm\,yr^{-1}}$ in the Brahmaputra mountains. Based on the respective mountain areas, this represents a mass increase of $0.8 \cdot 10^{12}\,\mathrm{kg\,yr^{-1}}$ in the Ganges catchment and $1.1 \cdot 10^{12}\,\mathrm{kg\,yr^{-1}}$ in the Brahmaputra catchment. However, this data could be biased by the station selection. Three of the stations from Xu et al. (2000) yield uplift rates around $20\,\mathrm{mm\,yr^{-1}}$. Removing these as outliers would reduce the mass change to $(1.5 \pm 0.3) \cdot 10^{12}\,\mathrm{kg\,yr^{-1}}$. One-third of this mass increase being located in the Ganges catchment and two-thirds being located in the Brahmaputra catchment.

In either case, gravity change associated with Himalayan uplift processes are in the same order of magnitude as those associated with sediment discharge and further studies should be conducted to better constrain their spatially resolved impact and potentially separate the impact of sediment discharge and Himalayan orogeny.

2 Description of the studied rivers

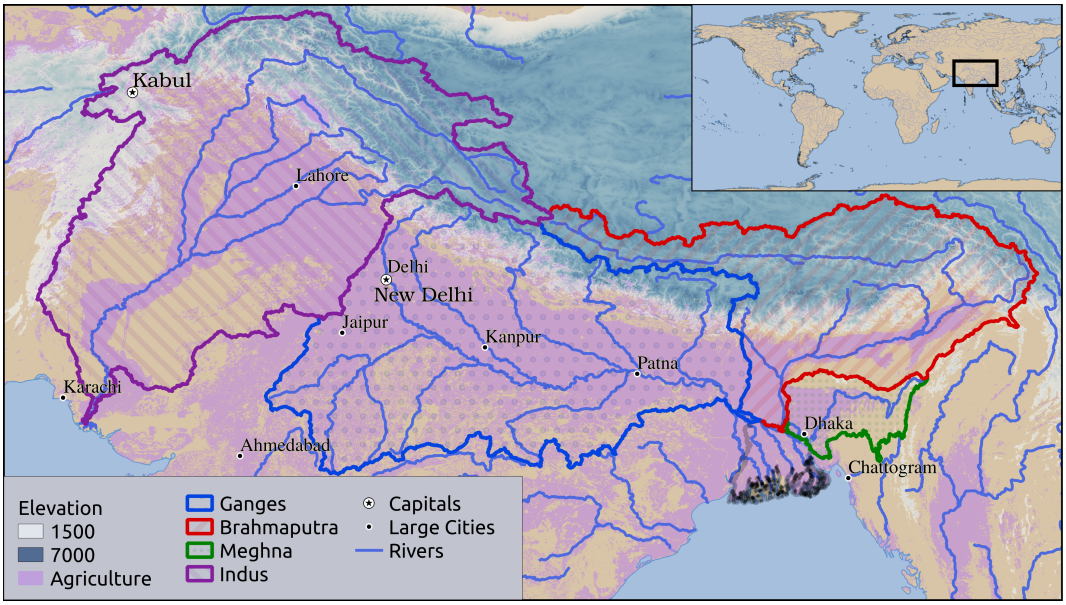

Figure S2. Map of investigated catchments and river paths as well as indicated areas of mountain (elevation $\geq 1{,}500\,\mathrm{m}$) and agricultural regions. Elevation data is from Jarvis et al. (2008), agriculture regions are from GLCNMO (2017), river paths are from GRDC (2020), and river catchments are from Lehner and Grill (2013).

2.1 The Ganges River

The Ganges River drains a basin of $950{,}754\,\mathrm{km}^2$ mainly located in India, but also including Nepal as well as parts of China and Bangladesh (Figure 1). The river originates at the Gangotri glacier ($7{,}010\,\mathrm{m}$ altitude) in the Uttaranchal Himalaya close to the Tibet-India border (Coleman, 1969; Singh, 1988), descends along the Great and Lesser Himalaya and flows southeast across India. In Bangladesh, it confluences with the Brahmaputra River to form the river Padma, which discharges into the Bay of Bengal (Figure 1, Figure S2). Prior to the 16th century, the majority of water from the Ganges discharged directly into the Bay of Bengal in the western part of the river delta. Over time, the channel migrated northeast to its present position (Coleman, 1969). The total length of the main Ganges River branch from its origin to the sea is about $2{,}507\,\mathrm{km}$ (Akhtar et al., 2009). The river profile shows an initial steep decline along the mountains, followed by about $2{,}000\,\mathrm{km}$ of little slope through the

Indo-Gangetic plain (Figure S3). The basin is bounded in the north by the Himalayas and in the south by the Vindhya Range (Singh, 1988).

2.2 The Brahmaputra River

The Brahmaputra River drains a basin of $539{,}989\,\mathrm{km}^2$ within the countries of China, India, Bhutan, and Bangladesh (Figure 1, Figure S2). It originates in Tibet on the north slope of the Himalayas and initially flows eastward to the eastern end of India, where it turns south and then west until it reaches Bangladesh, and confluences with the the Ganges River (Figure 1, Figure S2, Coleman, 1969). The Brahmaputra is a braided river that carries similar amounts of water to the Ganges River but slightly more sediment (Coleman, 1969). Generally flood peaks in the Brahmaputra will occur before the peaks in the Ganges (Coleman, 1969). The total length of the main Brahmaputra river branch is about $3{,}969\,\mathrm{km}$. In contrast to the Ganges river, its profile shows a slower decline along the mountain branch for about $2{,}000\,\mathrm{km}$ before the steeper decline when leaving the mountain regions and it only flows through floodplain regions for about $1{,}200\,\mathrm{km}$ before discharging into the ocean (Figure S3).

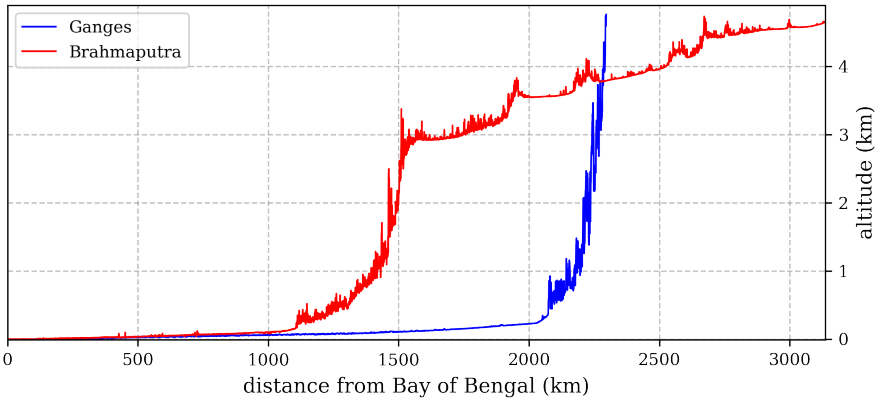

Figure S3. Profiles for the main branches of the Ganges and Brahmaputra rivers. Elevation is derived from data of Jarvis et al. (2008). River paths are as defined in GRDC (2020).

2.3 The Meghna River

The Meghna River is often considered in combination with the Ganges and Brahmaputra rivers. These three rivers confluence in Bangladesh (Figure 1, Figure S2) to form the Ganges-Brahmaputhra-Meghna Delta, the Earth's largest and most populous delta system (Paszkowski et al., 2021). However, in contrast to the Ganges and Brahmaputra rivers, which are rich in sediment, the Meghna river originates in the Indian Naga Hills at less than $2{,}000\,\mathrm{m}$ elevation and carries comparatively little sediment of $(6-12)\cdot 10^9\,\mathrm{kg\,yr}^{-1}$ (Rahman et al., 2018).

2.4 The Indus River

The Indus River originates in the northern slope of the Mount Kailash, close to the Brahmaputra River origin (Figure 1, Figure S2). It initially flows westwards and after partially circumventing the northern flanks of the Nanga Parbat-Haramosh Massif continues flowing to the southwest before discharging into the Arabian Sea (Figure 1, Figure S2, Inam et al., 2007). It is one of the Word's largest rivers and its sediment is mainly eroded from the western Tibetan plateau and Karakorum (Inam et al., 2007). Sediment discharge from the Indus River is smaller than from the Ganges and Brahmaputra rivers (Table 3). It has been estimated that before human intervention in the years 1950 to 1960, the Indus annually carried 300 to $675 \cdot 10^9$ kg of sediment of which about $250 \cdot 10^9$ kg reached the Indus Delta (Milliman et al., 1984). However, the installment of dams along the river reduced the annual sediment discharge by more than 80 % (Milliman and Meade, 1983; Giosan et al., 2006).

3 Challenges in data comparability and necessary assumptions

3.1 Scarcity in sediment measurements from the Indian subcontinent

Measurements of river sediment in the investigated rivers are scarce. We collected data from a variety of studies. However, most of those studies are based on data from sampling stations at the Hardinge Bridge (Ganges River, Table S2) and in Bahadurabad (Brahmaputra River, Table S3). Both of these stations are located after the rivers enter Bangladesh. Generally, sediment data are from river locations close to the delta region and no data from the upper rivers are available (Figure S4). Accordingly, the sediment discharge estimated for these stations yields an average mass loss for the catchments above those locations but no spatial resolution.

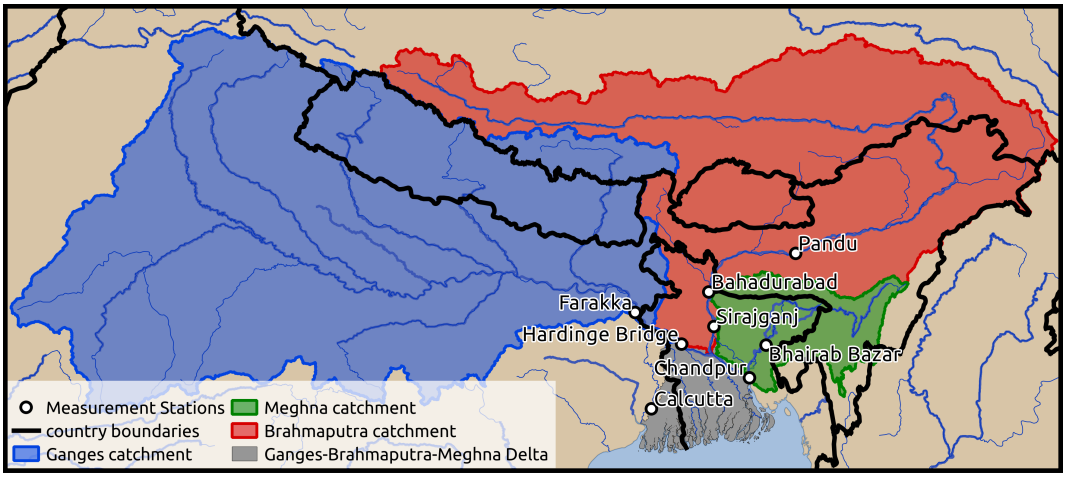

Figure S4. Map of Ganges-Brahmaputra-Meghna river system with locations of sediment study locations as stated in Table S2 and Table S3. River locations are from GRDC (2020) and river catchments are from Lehner and Grill (2013).

The river catchments are defined such that they exclude the river delta where a lot of sediment is deposited. This allows a good estimate of net sediment mass loss from the full river system as well as the individual catchments. When studying the mountain regions and floodplains individually, we are dependent on studies of the sediment origin (Faisal and Hayakawa, 2022; Garzanti et al., 2011; Galy et al., 2007; Wasson, 2003). However, those studies find the region where sediment initially originates from and do not provide information on potential deposition and re-distribution of sediment in the floodplains. Thus, the estimated origin fraction of net sediment mass loss does not necessarily translate to that amount of local mass loss. It is possible that sediment from the mountains is deposited in the floodplains, resulting in underestimation of mass loss in the mountains and overestimation of mass loss in the floodplains. The other way around, it is possible that large amounts of previously deposited mountain sediment is transported from the floodplains, resulting in overestimation of mountain sediment mass loss and an underestimation of floodplain sediment mass loss. Over long time periods, what we derive is likely a minimum estimate of sediment mass loss in the mountains and a maximum estimate of mass loss in the floodplains.

3.2 Potential impact of GRACE data filtering and leakage

To suppress GRACE data errors arising from instrument noise, modeling deficiencies and directional model sensitivity, the COST-G data we use are filtered spatially (Mu et al., 2017; Tripathi et al., 2022). This limits the resolution and causes data leakage between the individual grids (Figure S5). Thus, measured EWH loss from one catchment could falsely be attributed to neighboring ones. For the total study area of the combined Ganges, Brahmaputra, Meghna and Indus catchments, this impact is likely negligible. However, considering the main location of EWH loss in north-west India being located at the intersection between the Ganges and Indus catchments, this could yield an error in the attribution of this mass loss between the two catchments.

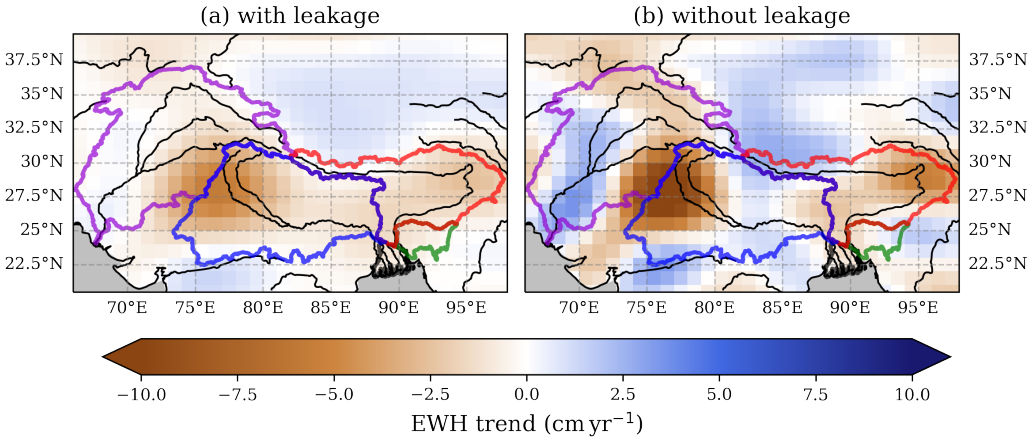

Figure S5. Map of the local equivalent water height (EWH) trends within the study area. (a) Including the leakage caused by filtering and (b) without the impact of leakage due to filtering. Data are from the COST-G Level 3 data product (Boergens et al., 2020).

Additionally, the data leakage softens the impact of local mass loss in individual grids which makes it impossible to observe and validate the potential sediment mass loss in the Namcha Barwa syntaxis within the GRACE TWS data. For proper data comparison between sediment mass loss and GRACE TWS, the GRACE filter would need to be applied to the sediment data. However, this would require gridded sediment loss data which are not available.

4 Regional analysis of TWS trends

The results of our study are based on linear trends in TWS and sediment mass loss. This section investigates the impact of changing seasonality and data gaps on such linear trends. We performed dynamic linear model fits on the regional monthly data using the dlmhelper Python package. Within the model fits, we allowed for variability in data seasonality and in data trend. We evaluated the trends for the best twelve results, whereat best refers to the lowest Akaike information criterion (AIC) value.

Resulting trends from the dynamic model, within their uncertainties, agree with the linear model trends (Table S1). For variable model trends, we derived average values over the GRACE time period. The dynamic model results are shown in Figure S10 - Figure S15. A full-on discussion of the trend variability is not included in this study since temporal comparison with the sediment data is not possible due to data scarcity. Accordingly we determined the linear least-squares approximation to be sufficient for the scope of our study.

Table S1. Trend analysis for individual catchments.

	linear model	dynamic model		
river	trend ($\mathrm{cm\,yr^{-1}}$)	trend ($\mathrm{cm\,yr^{-1}}$)	min ($\mathrm{cm\,yr^{-1}}$)	max ($\mathrm{cm\,yr^{-1}}$)
Total	-1.35 ± 0.07	-1.32 ± 0.04	-1.46	-1.32
GBM	-1.47 ± 0.12	-1.42 ± 0.13	-1.75	-1.27
Ganges	-1.60 ± 0.13	-1.52 ± 0.19	-1.95	-1.36
Brahmaputra	-1.41 ± 0.11	-1.41 ± 0.05	-1.42	-1.25
Meghna	-0.57 ± 0.24	-0.55 ± 0.06	-0.71	-0.53
Indus	-1.18 ± 0.05	-1.13 ± 0.07	-1.18	-1.03
Ganges-m	-1.51 ± 0.10	-1.47 ± 0.22	-1.95	-1.35
Brahmaputra-m	-1.57 ± 0.08	-1.58 ± 0.04	-1.58	-1.45

Linear model trend is the trend resulting from simple linear least-squares fits as applied in our study. Dynamic model trend refers to the results from data fits using the dlmhelper python package. The dynamic model trend, min, and max refer to the median, minimum, and maximum trend based on the twelve dynamic model fits that return the lowest AIC value. Uncertainty of the median trend is provided as standard deviation of such twelve values. Total refers to the combined Ganges, Brahmaputra, Meghna, and Indus catchments. GBM is the Ganges-Brahmaputra-Meghna catchment. Ganges-m and Barhmaputra-m refer to the mountain regions (altitude $\geq 1{,}500\,\mathrm{m}$) within the Ganges and Brahmaputra catchment, respectively.

5 Spatial resolution of sediment erosion

Due to data scarcity, it is difficult to spatially resolve sediment induced changes in gravity (see subsection 3.1). Here, we aim to generate such data based on modeled soil loss indexes from the Revised Universal Soil Loss Equation (RUSLE, Borrelli et al., 2017). These data provide estimates of global soil loss by water erosion based on inputs of rainfall, soil, topography, land use, and management at a spatial resolution of $25\,\mathrm{km}$ (Figure S6). For better comparison to the GRACE TWS data, soil loss data was re-gridded by taking average values for $1^\circ \times 1^\circ$ grid cells (Figure S6).

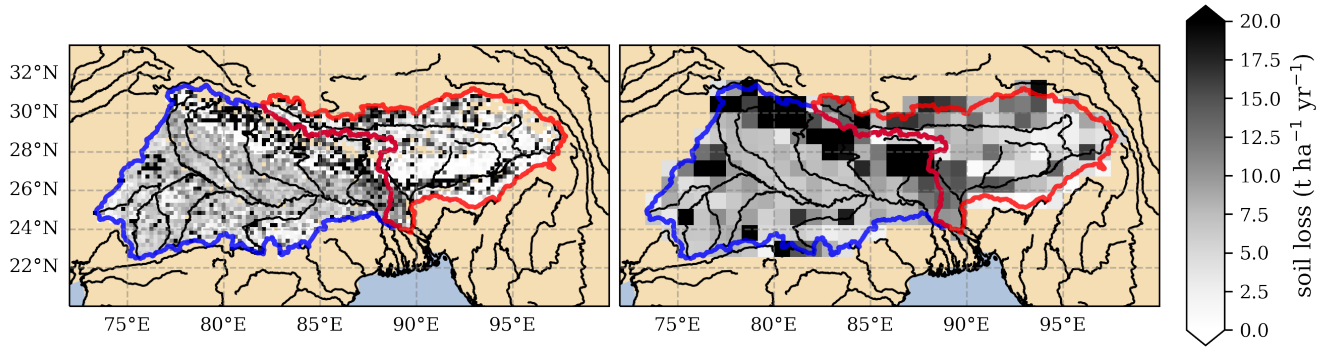

Figure S6. Map of regional soil loss in the Ganges and Brahmaputra catchments from Borrelli et al. (2017) in original resolution (left) and averaged for the TWS data resolution (right). The Ganges and Brahmaputra catchments are outlined in blue, and red, respectively.

These $1^\circ \times 1^\circ$ soil loss data were normalized and weighed by the sediment discharged of the individual rivers. Resulting sediment mass loss per grid cell were then divided by the cell's area and the water density to provide gridded sediment loss in terms of EWH (Figure S7). This process was performed in two ways. 1) the sediment discharge by the Ganges and Brahmaputra rivers were individually weighed by soil loss within the respective catchment area. 2) the total sediment discharge from the Ganges-Brahmaputra-Meghna River system was weighed by the soil loss in the combined catchments.

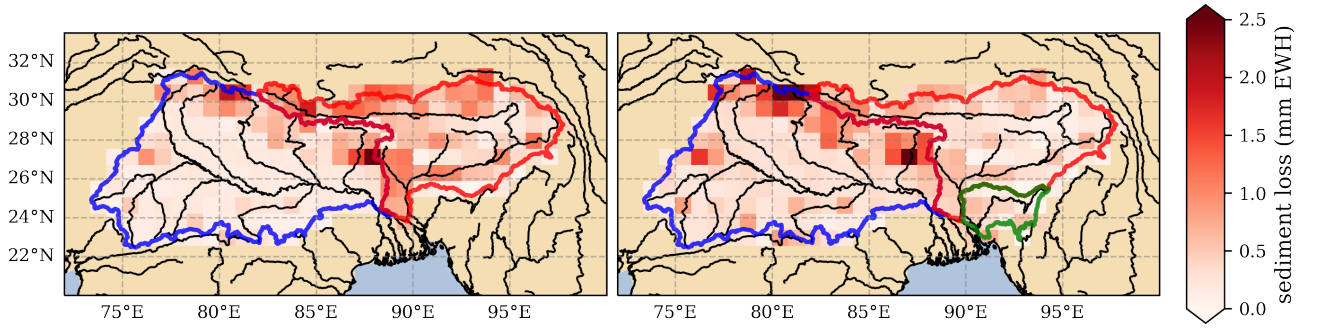

Figure S7. Map of regional sediment mass loss in terms of equivalent water height (EWH). River sediment discharges were weighed by soil loss data from Borrelli et al. (2017). First, Ganges and Brahmaputra discharges were individually weighed by soil loss within the respective catchment (left) and second, total sediment discharge from the Ganges-Brahmaputra-Meghna River system was weighed by the soil loss in the combined catchments (right). The Ganges, Brahmaputra, and Meghna catchments are outlined in blue, red, and green, respectively.

Weighing of the rivers individually yields high sediment loss in the Ganges mountains and fairly low and uniform sediment loss in the Ganges floodplains. In the Western Ganges region, there is one pixel of higher sediment erosion located within the region of strongest GRACE TWS trends. Yet, at mass loss of $\approx 1\,\mathrm{mm}$ EWH per year, it is significantly smaller than sediment loss in the Ganges mountains (Figure S7). However, based on this erosion potential, only $34\,\%$ of the Ganges sediment would be eroded from the mountains, while collective studies based on sediment composition and tracer experiments yield sediment fractions of $\approx 90\,\%$ being eroded from the Himalayas (Wasson, 2003; Faisal and Hayakawa, 2022).

In the Brahmaputra catchment, sediment erosion results to be distributed more uniformly than in the Ganges catchment, showing high sediment loss both in the mountain ranges and along the lower river path (Figure S7). The fraction of Brahmaputra sediment originated from the Himalayan mountains is therefore closely linked to the catchment's mountain fraction. Based on this erosion potential, it is $68\,\%$. Studies based on local measurements suggest a higher fraction of sediment being eroded from the mountain ranges (Wasson, 2003; Faisal and Hayakawa, 2022).

Weighing of sediment erosion over the total Ganges-Brahmaputra-Meghna catchment yields higher erosion rates in the Ganges catchment ($71\,\%$) than in the Brahmaputra catchment ($29\,\%$), while a total of $44\,\%$ are eroded from the mountain fraction (Figure S7). This higher sediment yield from the Ganges river agrees with data from Wasson (2003), while disagreeing with the more recent compilation of studies by Faisal and Hayakawa (2022).

In our study, we decided to follow the results by Faisal and Hayakawa (2022) and Wasson (2003) because they are based on local studies and sediment re-distribution along various pathways in the Ganges-Brahmaputra-Meghna river system complicate interpretation of the model based soil loss estimates presented here.

6 Interpretation of Indus data gap

In the Indus TWS time series, on first glance there appears to be an offset between data from the initial GRACE mission (before 07-2017) and the follow on mission GRACE-FO (after 05-2018, Figure S21). It appears that there is a weaker decline in the data than the linear optimization yields due to a jump to lower TWS during the data gap. However, both the GRACE and GRACE-FO data are calibrated to the same reference fields and should not contain an offset. We decided to look into the Indus catchment in more detail to investigate whether the generated trend is physically reasonable.

Investigation of individual catchment parts yield fairly constant TWS levels in the south-western and northern parts of the Indus catchment. In the northern mountains, there is a strong seasonality with only small inter-annual fluctuation. In the south-western catchment, the seasonality is much weaker, highlighting inter-annual events like the extreme flood in 2010. Neither of these regions show a significant trend or offset between data before and after the data gap (Figure S8). As shown in the TWS trend map (Figure 2), the main TWS decrease is located in the south-western part of the Indus catchment, where TWS steadily decreases. This decrease speeds up in 2016 and based on this data, a further TWS decrease during the measurement gap in 07-2017 to 05-2018 seems reasonable. The GRACE-FO data yields a fairly stagnant TWS levels until the end of 2020. We conclude that the observed trend, while in reality not being linear, seems physically reasonable and continue to use it in our study.

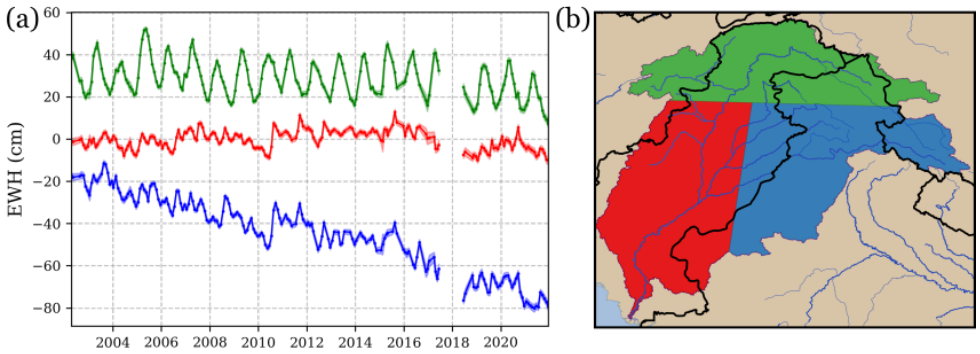

Figure S8. Equivalent water height (EWH) trends for different segments of the Indus catchment. (a) EWH trends for the northern (green), south-western (red), and south-eastern (blue) part of the Indus catchment. Data for the northern and south-eastern parts are adapted by an offset of $30\,\mathrm{cm}$ and $-40\,\mathrm{cm}$, respectively. (b) Map of the segment separation. A similar visualization for the Ganges catchment can be found in Figure S23.

7 Additional figures and tables

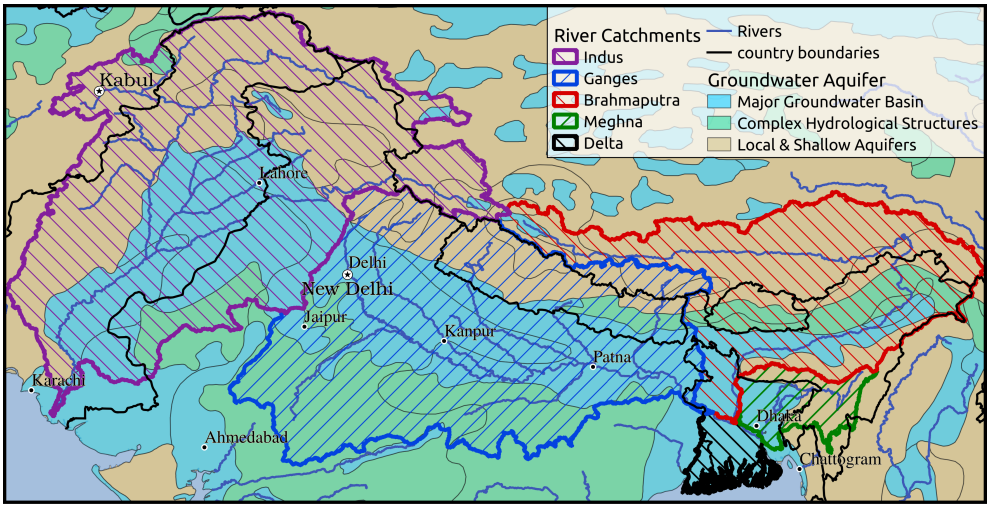

Figure S9. Map of study area with location and type of groundwater aquifers from EHYMAP RGWB (2010), river locations from GRDC (2020) and river catchments from Lehner and Grill (2013).

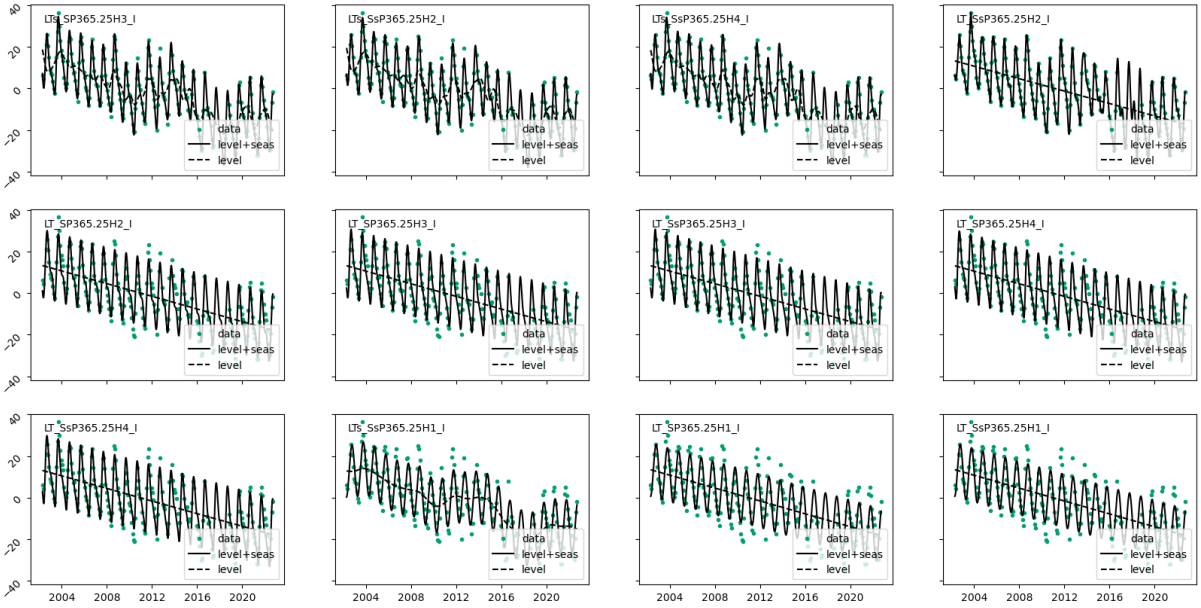

Figure S10. Results of dynamic linear model for the Ganges catchment region. Panels include the best 12 model results based on the AIC value.

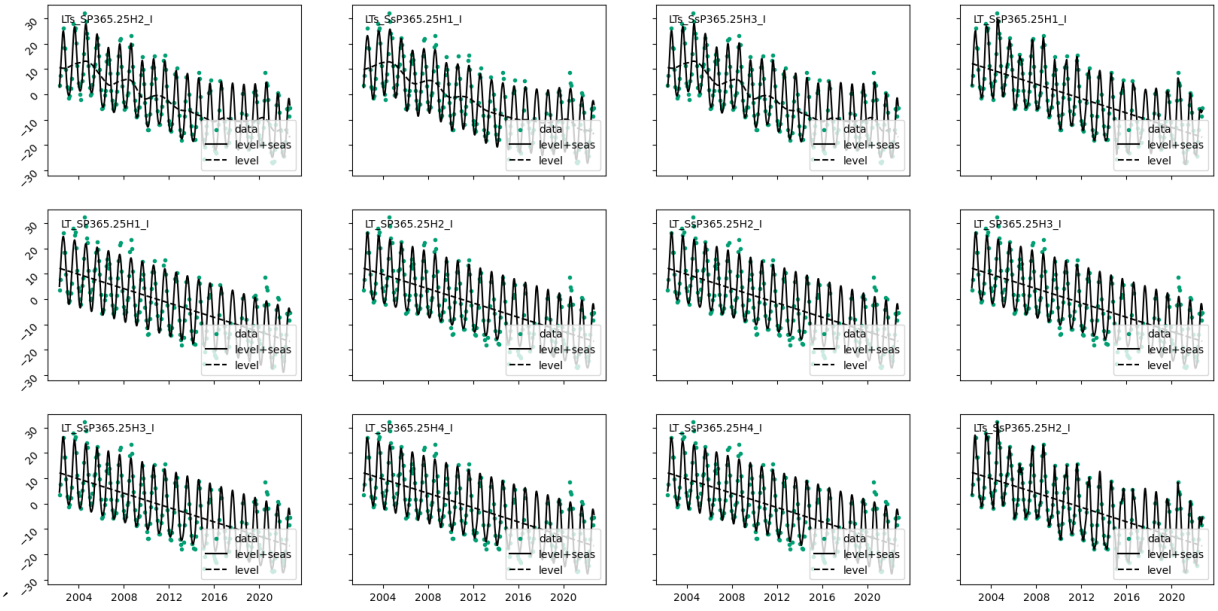

Figure S11. Results of dynamic linear model for the Brahmaputra catchment region. Panels include the best 12 model results based on the AIC value.

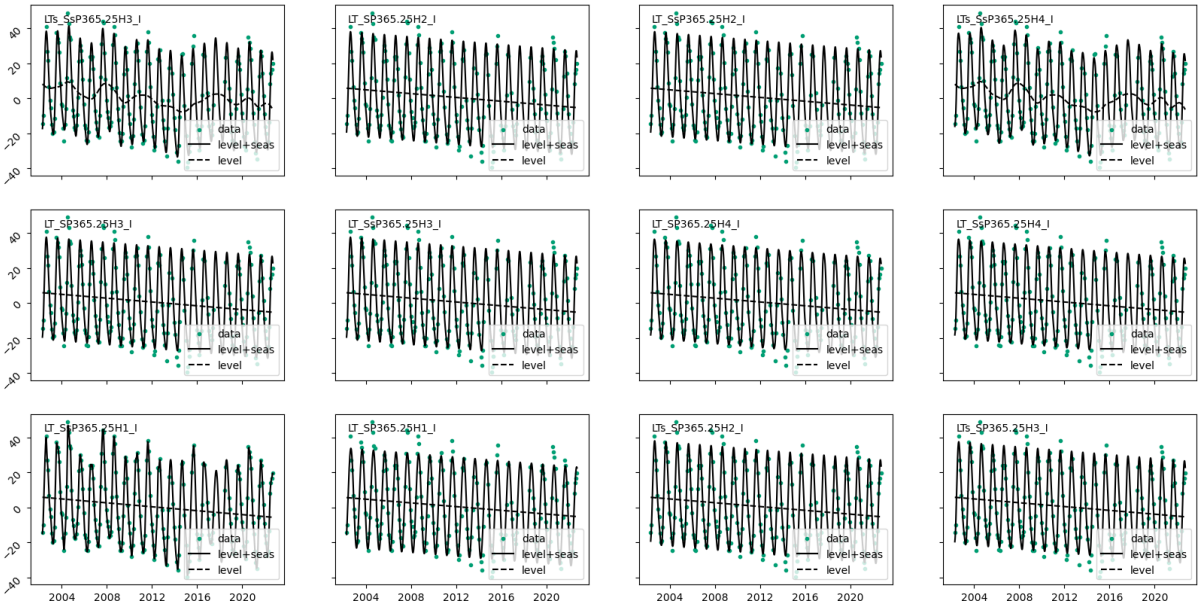

Figure S12. Results of dynamic linear model for the Meghna catchment region. Panels include the best 12 model results based on the the AIC value.

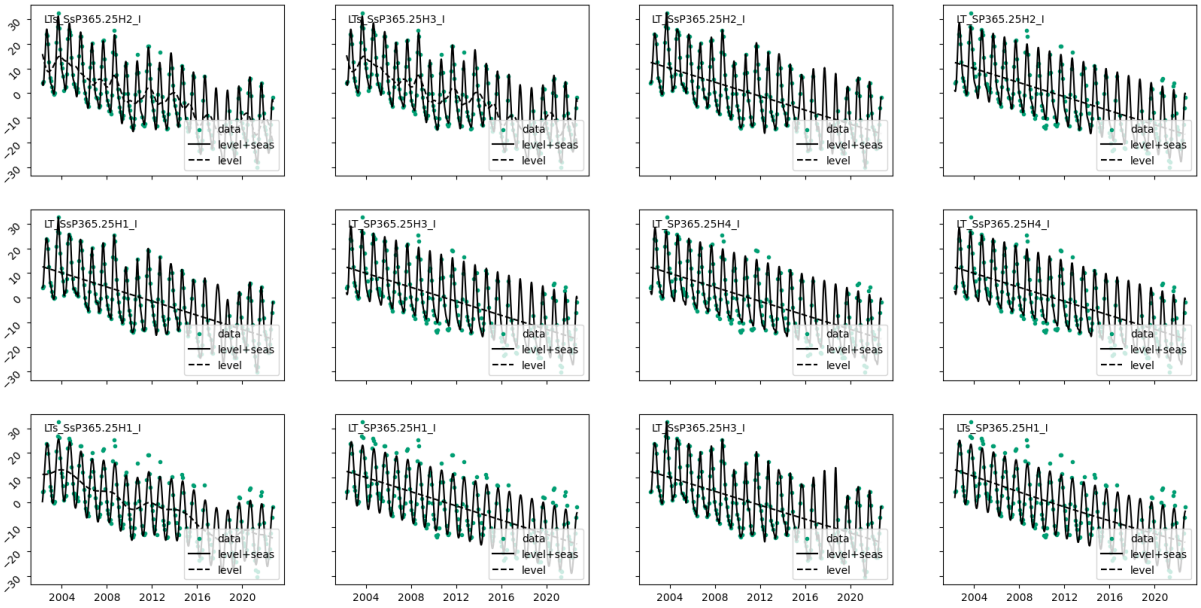

Figure S13. Results of dynamic linear model for the Ganges-Brahmaputra-Meghna catchment region. Panels include the best 12 model results based on the AIC value.

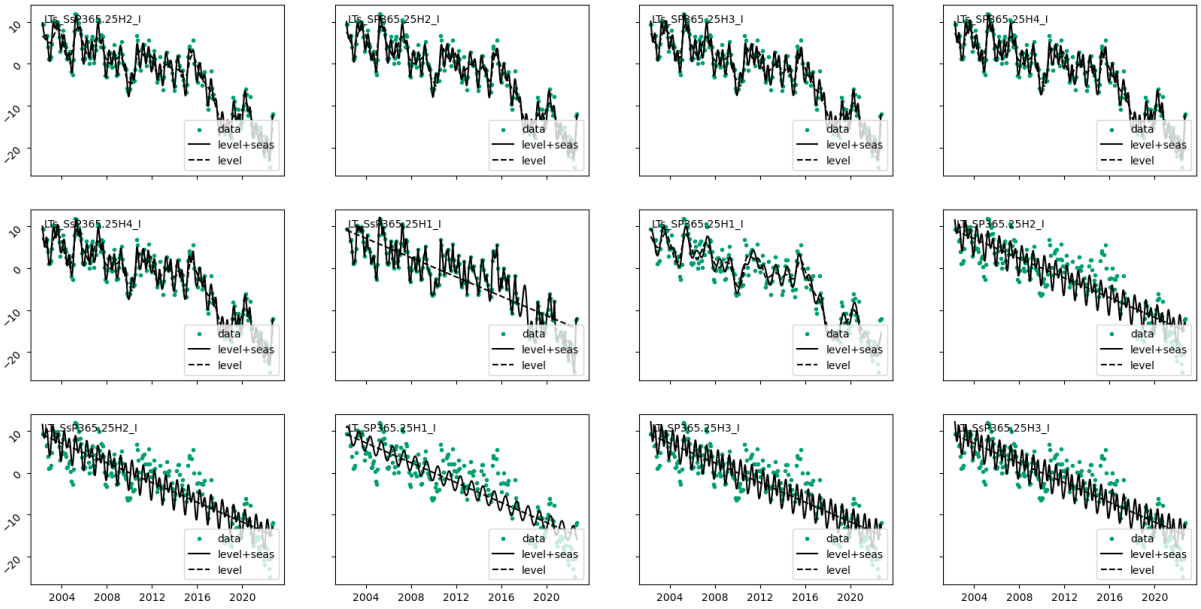

Figure S14. Results of dynamic linear model for the Indus catchment region. Panels include the best 12 model results based on the AIC value.

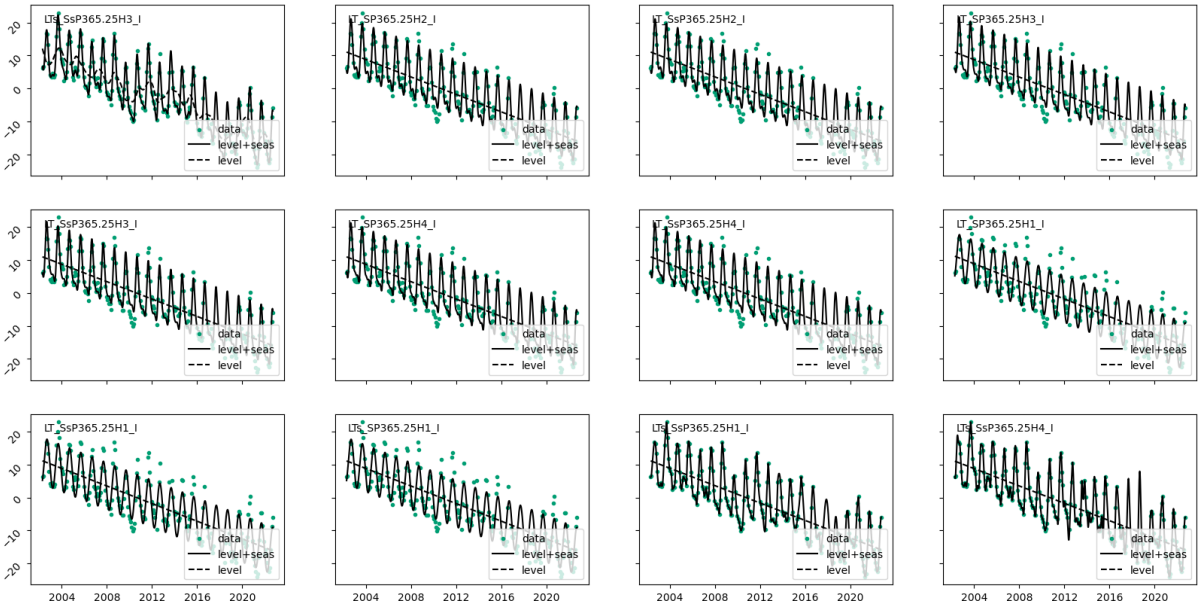

Figure S15. Results of dynamic linear model for the combined Ganges-Brahmaputra-Meghna and Indus catchment regions. Panels include the best 12 model results based on the AIC value.

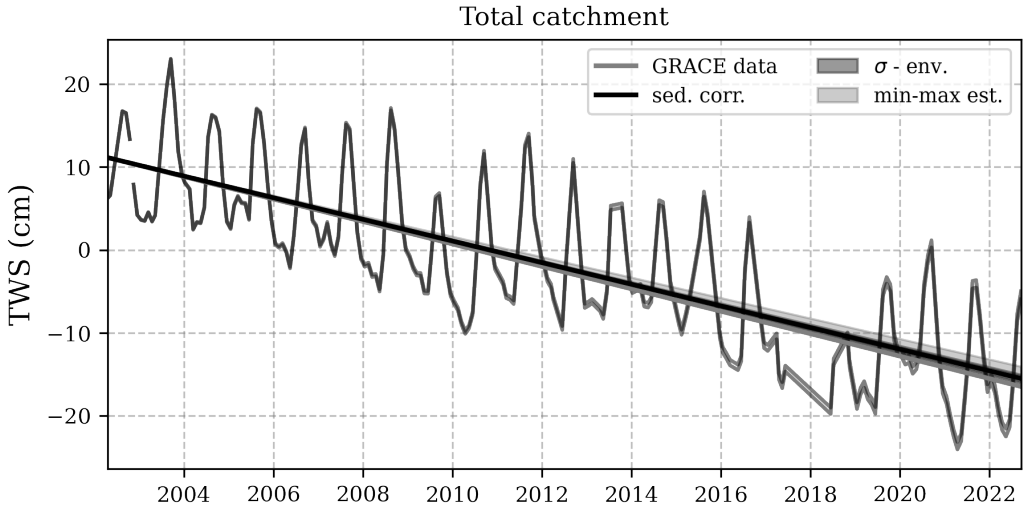

Figure S16. Time series of TWS derived from GRACE data (grey) and TWS corrected for sediment mass loss (black). Data show average over the whole Ganges, Brahmaputra, Meghna, and Indus catchments. Ranges for the σ-environment and the min-max estimates refer to the standard deviation as well as minimum and maximum estimates of sediment discharge as stated in Table 3.

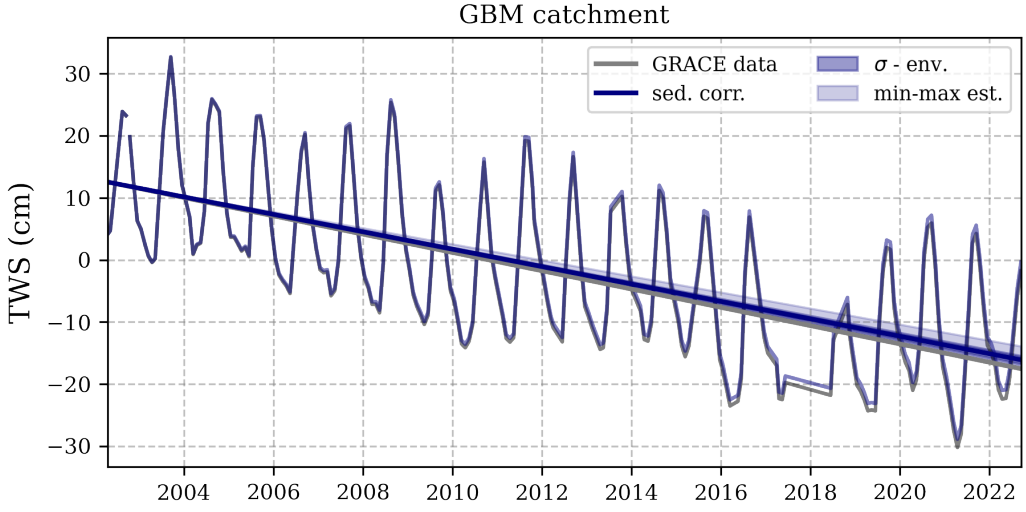

Figure S17. Time series of TWS derived from GRACE data (grey) and TWS corrected for sediment mass loss (blue). Data show average over the combined Ganges-Brahmaputra-Meghna catchment. Ranges for the σ-environment and the min-max estimates refer to the standard deviation as well as minimum and maximum estimates of sediment discharge as stated in Table 3.

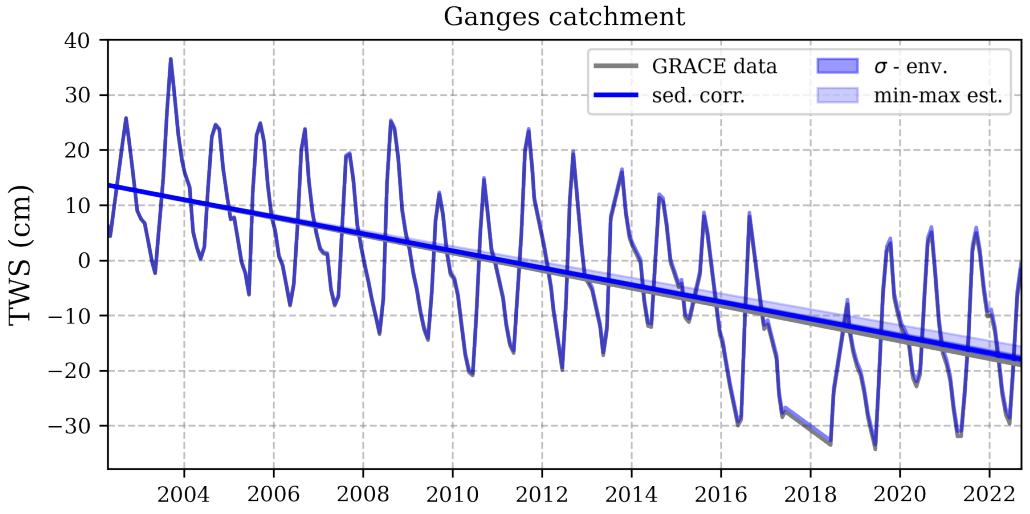

Figure S18. Time series of TWS derived from GRACE data (grey) and TWS corrected for sediment mass loss (blue). Data show average over the Ganges catchment. Ranges for the σ-environment and the min-max estimates refer to the standard deviation as well as minimum and maximum estimates of sediment discharge as stated in Table 3.

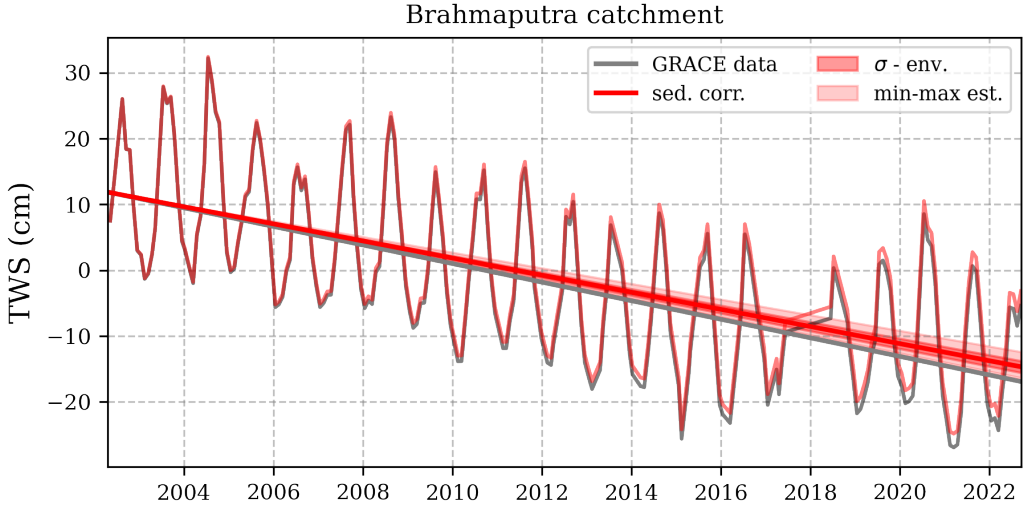

Figure S19. Time series of TWS derived from GRACE data (grey) and TWS corrected for sediment mass loss (red). Data show average over the Brahmaputra catchment. Ranges for the σ-environment and the min-max estimates refer to the standard deviation as well as minimum and maximum estimates of sediment discharge as stated in Table 3.

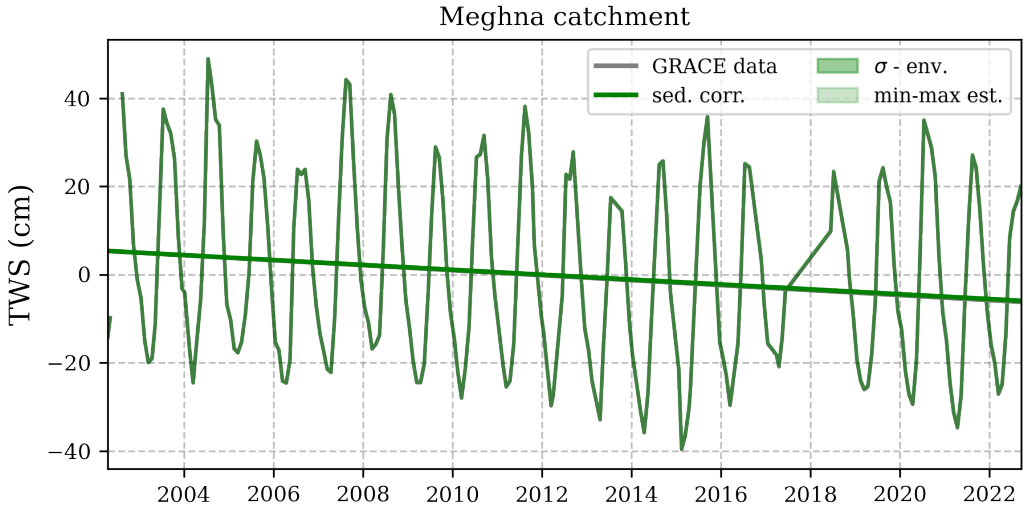

Figure S20. Time series of TWS derived from GRACE data (grey) and TWS corrected for sediment mass loss (green). Data show average over the Meghna catchment. Ranges for the σ-environment and the min-max estimates refer to the standard deviation as well as minimum and maximum estimates of sediment discharge as stated in Table 3.

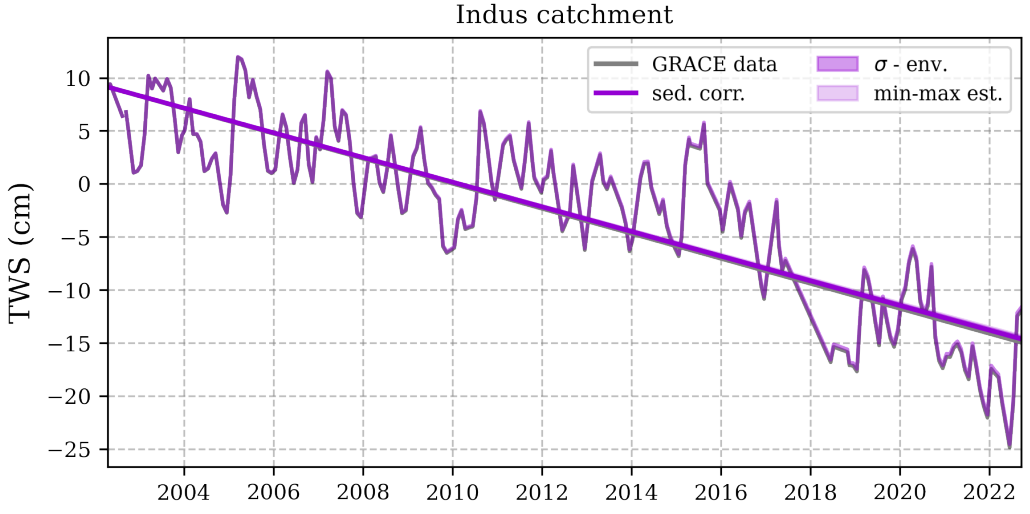

Figure S21. Time series of TWS derived from GRACE data (grey) and TWS corrected for sediment mass loss (purple). Data show average over the Indus catchment. Ranges for the σ-environment and the min-max estimates refer to the standard deviation as well as minimum and maximum estimates of sediment discharge as stated in Table 3.

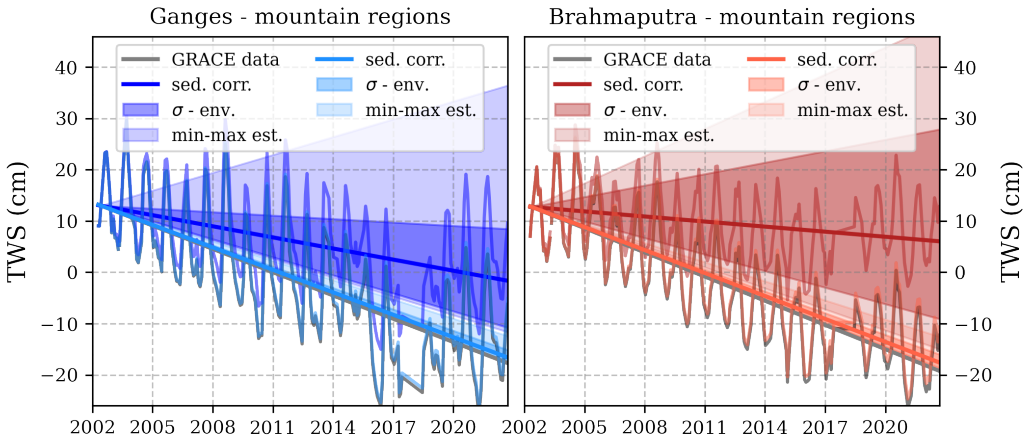

Figure S22. Time series of TWS derived from GRACE data (grey) and TWS after the correction for sediment mass loss (color). TWS data is derived as the average over the mountain fraction within the Ganges catchment (left) and the Brahmaputra catchment (right). For the Ganges catchment, the sediment correction is derived locally for the High Himalayas (HH, $\approx 57,976\,\mathrm{km}^2$) and the Lesser Himalayas (LH, $\approx 93,416\,\mathrm{km}^2$). These regions were defined analogous to Faisal and Hayakawa (2022). For the Brahmaputra catchment, the sediment correction is derived locally for the Namcha Barwa syntaxis (NBS, $\approx 21,600\,\mathrm{km}^2$) and the remaining mountain fraction (mount., $\approx 339,900\,\mathrm{km}^2$). Ranges for the σ-environment and the min-max estimates refer to the standard deviation as well as minimum and maximum estimates of sediment discharge as stated in Table 3.

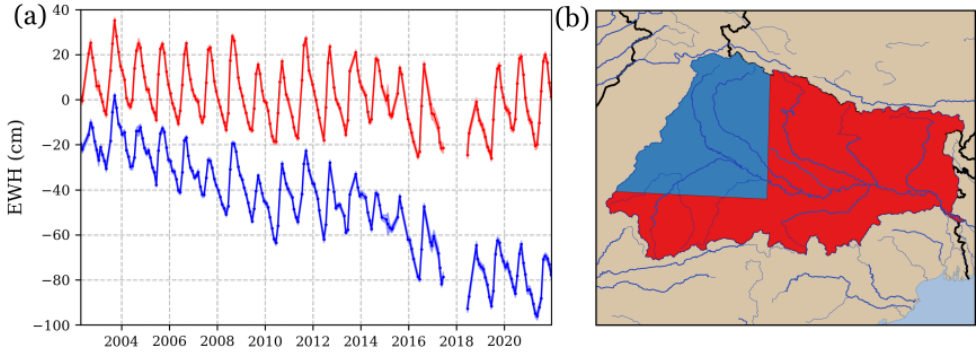

Figure S23. Equivalent water height (EWH) trends for different segments of the Ganges catchment. a) EWH trends for the north-western (blue), and south-eastern (red) part of the Ganges catchment. Data are adapted by an offset of $-42\,\mathrm{cm}$ and $2\,\mathrm{cm}$, respectively. b) Map of the catchment separation.

Table S2. Estimates of sediment load in the Ganges River from different literature studies.

susp. sediment (10^9 kg yr^{-1})	time period	location	source
210	unknown	Hardinge Bridge	MPO (1987) in Rahman et al. (2018)
340	unknown	Hardinge Bridge	FEC (1989) in Rahman et al. (2018)
430-729	unknown	unknown	Thakkar (2006)
550	unknown	unknown	CEGIS (2010) in Rahman et al. (2018)
1600	1874-1879	Hardinge Bridge	Holeman (1968)
478.9 (257-736)	1958-1962	Hardinge Bridge	Coleman (1969)
375	1960	unknown	NEDECO (1967) in Islam et al. (1999)
680$^{(a)}$	1966-1967	Hardinge Bridge	Milliman and Meade (1983)
520	1966-1969	Hardinge Bridge	BWDB (1972) in Islam et al. (1999)
548	1966-1970	Hardinge Bridge	WARPO (1996) in Rahman et al. (2018)
548	1966-1970	Hardinge Bridge	DH and DHI (1991) in Lupker et al. (2011)
200	1965-1988	Hardinge Bridge	CBJE (1991) in Rahman et al. (2018)
487	1976-1989	Hardinge Bridge	Tarekul Islam and Jaman (2006)
328	1981	Calcutta	Abbas and Subramanian (1984)
729	1981	Farakka	Abbas and Subramanian (1984)
403	1983-1984	Farakka	Singh (1988)
480 (350-600)	1980-1986	Hardinge Bridge	Hossain (1992) in Rahman et al. (2018)
502	1989-1991	Bengal Delta	Barua et al. (1994)
316 (155-863)	1979–1995	Hardinge Bridge	Islam et al. (1999)
216-1038	1981-2001	Hardinge Bridge	Akter et al. (2021)
150-590	1960-2008	Hardinge Bridge	Rahman et al. (2018)
262	2006	Hardringe Bridge	Rice (2007)
390 (360-420)	2004-2010	Hardinge Bridge	Lupker et al. (2011)

This set of estimates was build upon collections in Islam et al. (1999), Rahman et al. (2018) and Faisal and Hayakawa (2022). $^{(a)}$ Value for Ganges River taken from Islam et al. (1999). Original study states $1670 \cdot 10^9$ kg yr^{-1} after Ganges-Brahmaputra confluence.

Table S3. Estimates of sediment load in the Brahmaputra River from different literature studies.

Suspended sediment ($10^9\,\mathrm{kg\,yr^{-1}}$)	time period	location	source
390	unknown	unknown	MPO (1987) in Rahman et al. (2018)
800	unknown	unknown	Holeman (1968)
710	unknown	unknown	Subramanian (1987) in Islam et al. (1999)
430	unknown	Bahadurabad	FEC (1989) in FEC (1989)
590	unkown	unknown	CEGIS (2010) in Rahman et al. (2018)
402	1955-1979	Pandu	Goswami (1985)
607.7 (531-697)	1958-1962	Bahadurabad	Coleman (1969)
750	1960	unknown	NEDECO (1967) in Islam et al. (1999)
$1157^{(a)}$	1966-1967	Bahadurabad	Milliman and Meade (1983)
541	1966-1969	Bahadurabad	BWDB (1972) in Islam et al. (1999)
80-228	1981-2001	Bahadurabas	Akter et al. (2021)
500	1965-1988	Bahadurabad	CBJE (1991) in Rahman et al. (2018)
650 (400-850)	1980-1986	Bahadurabad	Hossain (1992) in Rahman et al. (2018)
1028	1989-1991	Bahadurabad	Barua et al. (1994)
721 (455-992)	1989–1994	Bahadurabad	Islam et al. (1999)
541	1993	Bahadurabad	Kabir and Ahmed (1996) in Rahman et al. (2018)
135-615	1960-2008	Bahadurabad	Rahman et al. (2018)
387	2006	Sirajganj	Rice (2007)

The set of estimates was build upon collections in Islam et al. (1999), Rahman et al. (2018) and Faisal and Hayakawa (2022)). $^{(a)}$Value for Brahmaputra River taken from Islam et al. (1999). Original study states $1670 \cdot 10^9\,\mathrm{kg\,yr^{-1}}$ after Ganges-Brahmaputra confluence.

Table S4. GPS uplift data within the Ganges and Brahmaputra Himalayan rage.

Uplift ($\mathrm{mm\,yr^{-1}}$)	latitude (°N)	longitude (°E)	source
6.84 ± 0.65	27.69	93.91	Bisht et al. (2021)
-4.3 ± 1.52	27.51	88.59	Bisht et al. (2021)
2.12 ± 0.37	29.68	79.65	Bisht et al. (2021)
-0.55 ± 0.36	29.47	79.57	Bisht et al. (2021)
-0.05 ± 0.01	30.33	78.82	Bisht et al. (2021)
0.65 ± 0.73	28.655	81.714	Fu and Freymueller (2012)
-1.5 ± 0.79	26.438	87.281	Fu and Freymueller (2012)
4.6 ± 0.37	28.207	85.314	Fu and Freymueller (2012)
2.16 ± 0.21	27.608	85.107	Fu and Freymueller (2012)
4.61 ± 0.55	28.983	82.817	Fu and Freymueller (2012)
1.08 ± 0.62	28.754	80.581	Fu and Freymueller (2012)
3.87 ± 0.68	29.733	80.5	Fu and Freymueller (2012)
2.61 ± 1.23	29.176	80.626	Fu and Freymueller (2012)
4.95 ± 0.58	27.95	82.491	Fu and Freymueller (2012)
6.07 ± 0.21	27.909	85.877	Fu and Freymueller (2012)
3.1 ± 0.73	29.277	82.192	Fu and Freymueller (2012)
3.79 ± 0.33	28.805	83.743	Fu and Freymueller (2012)
2.05 ± 0.29	27.8	85.278	Fu and Freymueller (2012)
1.25 ± 0.21	27.766	83.603	Fu and Freymueller (2012)
0.62 ± 0.27	29.657	91.104	Fu and Freymueller (2012)
2.04 ± 0.17	29.657	91.104	Fu and Freymueller (2012)
-2.14 ± 0.58	28.117	81.595	Fu and Freymueller (2012)
-1.29 ± 0.35	26.866	87.392	Fu and Freymueller (2012)
2.19 ± 1.16	26.99	86.597	Fu and Freymueller (2012)
-0.16 ± 0.33	27.165	84.985	Fu and Freymueller (2012)
3.9 ± 0.48	27.164	84.984	Fu and Freymueller (2012)
5.38 ± 0.64	29.969	81.806	Fu and Freymueller (2012)
0.94 ± 0.42	28.26	83.935	Fu and Freymueller (2012)
-1.92 ± 0.45	27.471	89.634	Fu and Freymueller (2012)
1.55 ± 0.32	27.352	87.709	Fu and Freymueller (2012)
2.3 ± 1	29.7	91.1	Xu et al. (2000)
7 ± 4.4	29.4	85.2	Xu et al. (2000)
6.6 ± 6.6	29.2	88.9	Xu et al. (2000)
19.2 ± 7.2	29.1	87.6	Xu et al. (2000)
17 ± 6.1	28.9	89.6	Xu et al. (2000)
22.1 ± 7.4	28.3	86	Xu et al. (2000)

References

Abbas, N. and Subramanian, V.: Erosion and sediment transport in the Ganges river basin (India), Journal of Hydrology, 69, 173–182, https://doi.org/10.1016/0022-1694(84)90162-8, 1984.

Akhtar, M. K., Corzo, G. A., van Andel, S. J., and Jonoski, A.: River flow forecasting with artificial neural networks using satellite observed precipitation pre-processed with flow length and travel time information: case study of the Ganges river basin, Hydrology and Earth System Sciences, 13, 1607–1618, https://doi.org/10.5194/hess-13-1607-2009, 2009.

Akter, J., Roelvink, D., and van der Wegen, M.: Process-based modeling deriving a long-term sediment budget for the Ganges-Brahmaputra-Meghna Delta, Bangladesh, Estuarine, Coastal and Shelf Science, 260, 107 509, https://doi.org/10.1016/j.ecss.2021.107509, 2021.

Barua, D. K., Kuehl, S. A., Miller, R. L., and Moore, W. S.: Suspended sediment distribution and residual transport in the coastal ocean off the Ganges-Brahmaputra river mouth, Marine Geology, 120, 41–61, https://doi.org/10.1016/0025-3227(94)90076-0, tidal and Shallow-Sea Sediments-Modern Environments, 1994.

Bisht, H., Kotlia, B. S., Kumar, K., Dumka, R. K., Taloor, A. K., and Upadhyay, R.: GPS derived crustal velocity, tectonic deformation and strain in the Indian Himalayan arc, Quaternary International, 575-576, 141–152, https://doi.org/https://doi.org/10.1016/j.quaint.2020.04.028, sI: Remote Sensing and GIS Applications in Quaternary Sciences, 2021.

Boergens, E., Dobslaw, H., and Dill, R.: COST-G GravIS RL01 Continental Water Storage Anomalies. V. 0004., GFZ Data Services., https://doi.org/10.5880/COST-G.GRAVIS_01_L3_TWS, accessed 20.12.2022, 2020.

Borrelli, P., Robinson, D. A., Fleischer, L. R., Lugato, E., Ballabio, C., Alewell, C., Meusburger, K., Modugno, S., Schütt, B., Ferro, V., Bagarello, V., Oost, K. V., Montanarella, L., and Panagos, P.: An assessment of the global impact of 21st century land use change on soil erosion., Nature Communications, 8, https://doi.org/10.1038/s41467-017-02142-7, data accessed 10.09.2023, 2017.

BWDB: Sediment investigations in Main Rivers of Bangladesh, 1968 & 1969, BWDB Water Supply Paper No. 359., (Bangladesh Water Development Board), 1972.

CBJE: Study Report on Flood Control and River Training Project on the Brahmaputra River in Bangladesh, Vol. 1 and Vol. 2, Government of Peoples Republic of China and Government of Bangladesh, Beijing and Dhaka, (China-Bangladesh Joint Expert Team), 1991.

CEGIS: Impact of Climate Change on Morphological Processes in Different River of Bangladesh, Prepared for Asian Development Bank, Dhaka, Bangladesh, (Center for Environmental and Geographic Information Services), 2010.

Coleman, J. M.: Brahmaputra river: Channel processes and sedimentation, Sedimentary Geology, 3, 129–239, https://doi.org/10.1016/0037-0738(69)90010-4, brahmaputra river: Channel processes and sedimentation, 1969.

DH and DHI: River Survey Project, Flood Action Plan 24, Water Resour. Plann. Org., Dhaka, (Delft Hydraulics and Danish Hydraulics Institute), 1991.

EHYMAP RGWB: River and Groundwater Basins of the World (WHYMAP RGWB) v1.0, The World-wide Hydrogeological Mapping and Assessment Programme (WHYMAP): River and Groundwater Basins of the World (RGWB), accessed via https://produktcenter.bgr.de/terraCatalog/OpenSearch.do?search=54e5d435-ac3f-4d2e-9e42-bd77728c1e05&type=/Query/OpenSearch.do (17.11.2022), 2010.

Faisal, B. M. R. and Hayakawa, Y. S.: Geomorphological processes and their connectivity in hillslope, fluvial, and coastal areas in Bangladesh: A review, Progress in Earth and Planetary Science, 9, https://doi.org/10.1186/s40645-022-00500-8, 2022.

FEC: Pre-Feasibility Study for Flood Control in Bangladesh, vol. 2, Present Conditions, Paris, (French Engineering Consortium), 1989.

Fu, Y. and Freymueller, J. T.: Seasonal and long-term vertical deformation in the Nepal Himalaya constrained by GPS and GRACE measurements, Journal of Geophysical Research: Solid Earth, 117, https://doi.org/https://doi.org/10.1029/2011JB008925, 2012.

Galy, V., France-Lanord, C., Beyssac, O., Faure, P., Kudrass, H., and Palhol, F.: Efficient organic carbon burial in the Bengal fan sustained by the Himalayan erosional system, Nature, 450, https://doi.org/10.1038/nature06273, 2007.

Garzanti, E., Andó, S., France-Lanord, C., Censi, P., Vignola, P., Galy, V., and Lupker, M.: Mineralogical and chemical variability of fluvial sediments 2. Suspended-load silt (Ganga–Brahmaputra, Bangladesh), Earth and Planetary Science Letters, 302, 107–120, https://doi.org/10.1016/j.epsl.2010.11.043, 2011.

Giosan, L., Constantinescu, S., Clift, P. D., Tabrez, A. R., Danish, M., and Inam, A.: Recent morphodynamics of the Indus delta shore and shelf, Continental Shelf Research, 26, 1668–1684, https://doi.org/10.1016/j.csr.2006.05.009, 2006.

GLCNMO: Global Land Cover by National Mapping Organizations: GLCNMO Version 3, Geospatial Information Authority of Japan, Chiba University and Collaborating Organizations, accessed via https://github.com/globalmaps/gm_lc_v3 (26.10.2022), 2017.

Goswami, D. C.: Brahmaputra River, Assam, India: Physiography, Basin Denudation, and Channel Aggradation, Water Resources Research, 21, 959–978, https://doi.org/10.1029/WR021i007p00959, 1985.

GRDC: Major River Basins of the World: "Major Rivers", Global Runoff Data Centre. 2nd, rev. ext. ed. Koblenz, Germany: Federal Institute of Hydrology (BfG), accessed via: https://www.bafg.de/SharedDocs/ExterneLinks/GRDC/mrb_shp_zip.html;jsessionid=993792470F4B2723B3942ACFA8C09C66.live11313?nn=201762 (24.10.2022)., 2020.

Holeman, J. N.: The Sediment Yield of Major Rivers of the World, Water Resources Research, 4, 737–747, https://doi.org/10.1029/WR004i004p00737, 1968.

Hossain, M.: Total sediment load in the lower Ganges and Jamuna, J. Inst. Engrs. Bangladesh, 20, 1 – 8, https://www.scopus.com/inward/record.uri?eid=2-s2.0-0342490796&partnerID=40&md5=822d0234ae1a00fb7f29cd21c2f7e563, 1992.

Inam, A., Clift, P. D., Giosan, L., Tabrez, A. R., Tahir, M., Rabbani, M. M., and Danish, M.: The Geographic, Geological and Oceanographic Setting of the Indus River, chap. 16, pp. 333–346, John Wiley & Sons, Ltd, https://doi.org/10.1002/9780470723722.ch16, 2007.

Islam, M. R., Begum, S. F., Yamaguchi, Y., and Ogawa, K.: The Ganges and Brahmaputra rivers in Bangladesh: basin denudation and sedimentation, Hydrological Processes, 13, 2907–2923, https://doi.org/10.1002/(SICI)1099-1085(19991215)13:17<2907::AID-HYP906>3.0.CO;2-E, 1999.

Jarvis, A., Reuter, H., Nelson, A., and Guevara, E.: Hole-filled seamless SRTM data V4, International Centre for Tropical Agriculture (CIAT), accessed from https://srtm.csi.cgiar.org (24.10.2022)., 2008.

Kabir, M. and Ahmed, N.: Bed shear stress for sediment transportation in the River Jamuna, Journal of Civil Engineering, The Institution of Engineers, Bangladesh, 24 CE, 55 – 68, https://www.scopus.com/inward/record.uri?eid=2-s2.0-84892444734&partnerID=40&md5=1d4dbda20f2a153bd21c6a1f58db1348, 1996.

Larson, K. M., Bürgmann, R., Bilham, R., and Freymueller, J. T.: Kinematics of the India-Eurasia collision zone from GPS measurements, Journal of Geophysical Research: Solid Earth, 104, 1077–1093, https://doi.org/https://doi.org/10.1029/1998JB900043, 1999.

Lehner, B. and Grill, G.: Global river hydrography and network routing: baseline data and new approaches to study the world's large river systems., https://doi.org/10.1002/hyp.9740, accessed via https://www.hydrosheds.org/products/hydrobasins (20.10.2022), 2013.

Lupker, M., France-Lanord, C., Lavé, J., Bouchez, J., Galy, V., Métivier, F., Gaillardet, J., Lartiges, B., and Mugnier, J.-L.: A Rouse-based method to integrate the chemical composition of river sediments: Application to the Ganga basin, Journal of Geophysical Research: Earth Surface, 116, https://doi.org/10.1029/2010JF001947, 2011.

Milliman, J., Quraishee, G., and Beg, M.: Sediment discharge from the Indus River to the ocean: past, present and future, Marine geology and oceanography of Arabian Sea and coastal Pakistan, pp. 65–70, 1984.

Milliman, J. D. and Meade, R. H.: World-Wide Delivery of River Sediment to the Oceans, The Journal of Geology, 91, 1–21, http://www.jstor.org/stable/30060512, 1983.

MPO: Floods and storms, Tech. Rep. 11, (Master Plan Organization), 1987.

Mu, D., Yan, H., Feng, W., and Peng, P.: GRACE leakage error correction with regularization technique: case studies in Greenland and Antarctica, Geophysical Journal International, 208, 1775–1786, https://doi.org/10.1093/gji/ggw494, 2017.

NEDECO: East Pakistan Inland Water Transport Authority: Surveys of Inland Waterways and Ports 1963–1967, Hydrographic Manual, (Netherlands Engineering Consultants), 1967.

Paszkowski, A., Goodbred, S., Borgomeo, E., Khan, M. S. A., and Hall, J. W.: Geomorphic change in the Ganges–Brahmaputra–Meghna delta, Nature Reviews Earth & Environment, 2, https://doi.org/10.1038/s43017-021-00213-4, 2021.

Rahman, M., Dustegir, M., Karim, R., Haque, A., Nicholls, R. J., Darby, S. E., Nakagawa, H., Hossain, M., Dunn, F. E., and Akter, M.: Recent sediment flux to the Ganges-Brahmaputra-Meghna delta system, Science of The Total Environment, 643, 1054–1064, https://doi.org/10.1016/j.scitotenv.2018.06.147, 2018.

Rao, S. E., Ray, L., Khan, T., and Ravi, G.: Thermal conductivity, density and porosity of sedimentary and metamorphic rocks from the Lower and Higher Himalaya, Western Himalaya, India, Geophysical Journal International, 231, 459–473, https://doi.org/10.1093/gji/ggac176, 2022.

Ravikumar, M., Singh, B., Pavan Kumar, V., Satyakumar, A. V., Ramesh, D. S., and Tiwari, V. M.: Lithospheric Density Structure and Effective Elastic Thickness Beneath Himalaya and Tibetan Plateau: Inference From the Integrated Analysis of Gravity, Geoid, and Topographic Data Incorporating Seismic Constraints, Tectonics, 39, e2020TC006 219, https://doi.org/https://doi.org/10.1029/2020TC006219, e2020TC006219 2020TC006219, 2020.

Rice, S. K.: Suspended Sediment Transport in the Ganges-Brahmaputra River System, Bangladesh, Master's thesis, Texas A & M University, 2007.

Singh, S. K.: Nature of chemical and sediment load in the Ganges River between Sone and Kosi, Ph.D. thesis, Jawaharlal Nehru University, New Delhi, India, http://hdl.handle.net/10603/16314, 1988.

Subramanian, V.: Environmental geochemistry of Indian river basins - a review., Journal of the Geological Society of India, 29, 205 – 220, https://www.scopus.com/inward/record.uri?eid=2-s2.0-0023159471&partnerID=40&md5=9ef05ffa095d623bcc21a195a1f8ea24, 1987.

Tarekul Islam, G. M. and Jaman, S. T.: Modelling sediment loads in the Lower Ganges, Bangladesh, Proceedings of the Institution of Civil Engineers - Water Management, 159, 87–94, https://doi.org/10.1680/wama.2006.159.2.87, 2006.

Thakkar, H.: What, who, how and when of experiencing floods as a disaster, Issues, 20, 1 – 37, https://www.scopus.com/inward/record.uri?eid=2-s2.0-84920029256&partnerID=40&md5=5ad08ce56e55b9346fd5fd67df83df0d, 2006.

Tripathi, V., Groh, A., Horwath, M., and Ramsankaran, R.: Scaling methods of leakage correction in GRACE mass change estimates revisited for the complex hydro-climatic setting of the Indus Basin, Hydrology and Earth System Sciences, 26, 4515–4535, https://doi.org/10.5194/hess-26-4515-2022, 2022.

WARPO: Sediment Rating Curves and Balances, Special Report No. 18 River Survey Project, Dhaka, Bangladesh, (Water Resources Planning Organization), 1996.

Wasson, R. J.: A sediment budget for the Ganga–Brahmaputra catchment, Current Science, 84, 1041–1047, http://www.jstor.org/stable/24107666, 2003.

Xu, C., Liu, J., Song, C., Jiang, W., and Shi, C.: GPS measurements of present-day uplift in the Southern Tibet, Earth, Planets and Space, 52, 735–739, https://doi.org/10.1186/BF03352274, 2000.